Supplemental Information for:

On the contribution of nocturnal heterogeneous reactive nitrogen chemistry to particulate matter formation during wintertime pollution events in Northern Utah

Erin E. McDuffie[1,2,3ξ], Caroline Womack[1,2], Dorothy L. Fibiger[1,2†], William P. Dube[1,2], Alessandro Franchin[1,2], Ann Middlebrook[1], Lexie Goldberger[4‡], Ben H. Lee[4], Joel A. Thornton[4], Alexander Moravek[5], Jennifer Murphy[5], Munkhbayar Baasandorj[6§], Steven S. Brown[1,3]

[1]Chemical Sciences Division, National Oceanic and Atmospheric Administration, Boulder, CO, USA
[2]Cooperative Institute for Research in Environmental Sciences, University of Colorado, Boulder, CO, USA
[3]Department of Chemistry, University of Colorado, Boulder, CO, USA
[4]Department of Atmospheric Science, University of Washington, Seattle, WA, USA
[5]Department of Chemistry, University of Toronto, Toronto, Canada
[6]Department of Atmospheric Sciences, University of Utah, Salt Lake City, UT, USA

[ξ]Now at: Department of Physics and Atmospheric Science, Dalhousie University, Halifax, NS, Canada
†Now at: California Air Resources Board, Sacramento, CA, USA
‡Now at: ARM Aerial Facility, Pacific Northwest National Laboratory, Richland, WA, USA
§Now at: Chevron Corporation, Houston, TX, USA

Correspondence to: Steven S. Brown (steven.s.brown@noaa.gov)

Contents:

Pages: 12

Sections: S1-S4

Figures: S1- S5

Tables: S1-S4

Section S1 Additional Model Details

S1.1 Model Chemical Mechanism

Table S1. Box Model Chemical Mechanism and Reactions used in Sensitivity Simulations

Reactants	Products	Rate Coefficient Expression	Reference/ Source
NO_2+O_3	→ $NO_3 + O_2$	$k_1 = 1.4\times10^{-13} e^{(-2470/T)}$ [cm^3 $molec.^{-1}$ s^{-1}]	IUPAC 2008
$NO_3 + NO_2$	→ N_2O_5	$k_{2f} = (k0/k\infty)*F/(k0+k\infty)$ [cm^3 $molec.^{-1}$ s^{-1}][a]	IUPAC 2012
N_2O_5	→ $NO_3 + NO_2$	$k_{2r} = (k0/k\infty)*F/(k0+k\infty)$ [cm^3 $molec.^{-1}$ s^{-1}][b]	IUPAC 2012
N_2O_5 + aerosol	→ 2 HNO_3	$k_3 = k_{HNO_3}$ [s^{-1}]	Derived
N_2O_5 + aerosol	→ $HNO_3 + ClNO_2$	$k_4 = k_{ClNO_2}$ [s^{-1}]	Derived
NO_3 + VOC	→ $RONO_2$	$k_5 = k_{NO_3}$ [s^{-1}]	Calculated[c]
NO_3 + NO	→ 2 NO_2	$k_6 = 1.80\times10^{-11} e^{(110/T)}$ [cm^3 $molec.^{-1}$ s^{-1}]	IUPAC 2008
NO + O_3	→ $NO_2 + O_2$	$k_7 = 2.07\times10^{-12} e^{(-1400/T)}$ [cm^3 $molec.^{-1}$ s^{-1}]	IUPAC 2013
O_3 + hν	→ $O + O_2$	k_8 = j(O^1D)	WINTER[c]
NO_2 + hν	→ NO + O	k_9 = j(NO_2)	WINTER[c]
NO_3 + hν	→ NO_2 + O	k_{10} = j(NO_3)	WINTER[c]
N_2O_5 + hν	→ $NO_2 + NO_3$	k_{11} = j(N_2O_5)	WINTER[c]
$ClNO_2$ + hν	→ Cl + NO_2	k_{12} = j($ClNO_2$)	WINTER[c]
Styrene + NO_3	→ $RONO_2$	$k_{NO_3} = 1.5\times10^{-12}$ [s^{-1}]	k_{NO_3} case[d]
∑(*cis*, *trans*-2-Butene) + NO_3	→ $RONO_2$	$k_{NO_3} = 3.7\times10^{-13}$ [s^{-1}]	k_{NO_3} case[d]
∑(*cis*, *trans*-2-Pentene) + NO_3	→ $RONO_2$	$k_{NO_3} = 3.7\times10^{-13}$ [s^{-1}]	k_{NO_3} case[d]
Isoprene + NO_3	→ $RONO_2$	$k_{NO_3} = 3.15\times10^{-12}*\exp^{(-450/T)}$ [s^{-1}]	k_{NO_3} case[d]
N_2O_5	→	$k_{Dilution} = 1.3\times10^{-6}$ [s^{-1}]	$k_{Dilution}$ case[e]
$ClNO_2$	→	$k_{Dilution} = 1.3\times10^{-6}$ [s^{-1}]	$k_{Dilution}$ case[e]
NO_2	→	$k_{Dilution} = 1.3\times10^{-6}$ [s^{-1}]	$k_{Dilution}$ case[e]
HNO_3	→	$k_{Dilution} = 1.3\times10^{-6}$ [s^{-1}]	$k_{Dilution}$ case[e]
NO_3	→	$k_{Dilution} = 1.3\times10^{-6}$ [s^{-1}]	$k_{Dilution}$ case[e]
NO	→	$k_{Dilution} = 1.3\times10^{-6}$ [s^{-1}]	$k_{Dilution}$ case[e]
O_3	→	$k_{Dilution} = 1.3\times10^{-6}$ [s^{-1}]	$k_{Dilution}$ case[e]
O_3 Bkg[f]	→ O_3	$k_{Dilution} = 1.3\times10^{-6}$ [s^{-1}]	$k_{Dilution}$ case[e]

[a] $k_0 = 3.6\times10^{-30}*M*(T/300)^{-4.1}$, $k_\infty = 1.9\times10^{-12}*(T/300)^{0.2}$, KR = k_0/k_∞ NC = 0.75-1.27*$\log_{10}(0.35)$, F = $10^{(\log10(0.35)/(1+\log10(KR)/NC)^2))}$, M = Pressure [mbar] $1\times10^{-4}/(k_b*T)$

[b] $k_0 = 1.3\times10^{-3}*M*(T/300)^{-3.5}e^{(-11000/T)}$, $k_\infty = 9.7\times10^{14}*(T/300)^{0.1}e^{(-11080/T)}$, KR = k_0/k_∞ NC = 0.75-1.27*$\log_{10}(0.35)$, F = $10^{(\log10(0.35)/(1+\log10(KR)/NC)^2))}$, M = Pressure [mbar] $1\times10^{-4}/(k_b*T)$

[c] Described in Section S1.4.3, from the WINTER campaign

[d] Described in Sections S1.2 and S1.4.5, used only to test the sensitivity to time-varying NO_3 reactivity; rate constants from Atkinson and Arey (2003)

[e] Described in Section S1.4.1, used only in simulations that included air parcel dilution/vertical mixing

[f] Background O_3 = 45 ppbv

S1.2 NO_3 Reactivity Calculation Details

The values of the k_{NO_3} reaction rate constants for simulations of each flight were calculated from multiple ground-based VOC measurements as described below.

As noted in the main text, a set of select (< 20) VOCs were measured by a PTR-MS with hourly time resolution during UWFPS at a ground site on the University of Utah campus (Table S2). During 2012-2014, a larger set of > 45 VOCs was collected with hourly time resolution at the HW ground site and analyzed with a Gas-Chromatography Flame Ionization Detector. For calculations of k_{NO_3} here, concentrations of VOCs during UWFPS were estimated by applying the average 2012-2014 VOC:benzene ratio (from December – March data) to PTR-MS benzene concentrations observed in 2017, as described in Text S1

of Womack et al. (2018). Benzene was chosen as both benzene and toluene were the least reactive of the five compounds that were reported in both the historical data set and during the 2017 campaign. The toluene:benzene ratio derived from historical data (Table S2) reproduced the 2017 toluene concentrations within 3%, but the benzene:toluene ratio could only reproduce the 2017 concentrations of benzene by 30%. Applying the historical VOC:benzene ratios, estimates of 2017 VOC concentrations were used in Eq. (S1) to calculate total k_{NO_3} for all the simulations of 2017 flights. A complete list of measured/estimated VOC concentrations, their reaction rate constants (k_{VOC}), average historical VOC:benzene ratios, and measurement years are provided in Table S2.

$$k_{NO_3} = \sum([\mathrm{VOC}]_i * k_{VOC_i}) \quad \text{(S1)}$$

Table S2. NO_3 + VOC Reaction Rate Constants

VOC	A Factor (10^{14} cm^3 s^{-1})	B Factor (n)	Reference	VOC: benzene	Meas. Year
Alkanes					
CH_4	0.0001	0	(Atkinson & Arey, 2003)		2017
Ethane	0.0001	0	(Atkinson & Arey, 2003)	26.15	2012-2014
Propane	0.007	0	(Atkinson & Arey, 2003)	14.82	2012-2014
iso-Butane	305	3060	(Atkinson & Arey, 2003)	1.87	2012-2014
n-Butane	276	3279	(Atkinson & Arey, 2003)	5.48	2012-2014
2,2-Dimethylbutane	0.044	0	Estimated	0.03	2012-2014
2,3-Dimethylbutane	0.044	0	(Atkinson & Arey, 2003)	0.27	2012-2014
iso-Pentane	299	2927	(Atkinson & Arey, 2003)	2.41	2012-2014
n-Pentane	0.0087	0	(Atkinson & Arey, 2003)	2.17	2012-2014
2-Methyl Pentane	0.018	0	(Atkinson & Arey, 2003)	0.24	2012-2014
3-Methyl Pentane	0.022	0	(Atkinson & Arey, 2003)	0.01	2012-2014
n-Hexane	0.011	0	(Atkinson & Arey, 2003)	1.1	2012-2014
2-Methylhexane	0.015	0	Estimated	0.30	2012-2014
3-Methylhexane	0.015	0	Estimated	0.31	2012-2014
n-Heptane	0.015	0	(Atkinson & Arey, 2003)	0.49	2012-2014
n-Octane	0.019	0	(Atkinson & Arey, 2003)	0.11	2012-2014
n-Nonane	0.023	0	(Atkinson & Arey, 2003)	0.07	2012-2014
n-Decane	0.028	0	(Atkinson & Arey, 2003)	0.047	2012-2014
n-Undecane	0.032	0	Estimated	0.035	2012-2014
n-Dodecane	0.036	0	Estimated	0.02	2012-2014
Cyclohexane	0.014	0	(Atkinson & Arey, 2003)	0.40	2012-2014
Alkenes					
Ethene	0.000488	2282 (2)	(Atkinson & Arey, 2003)	9.35	2012-2014
Propene	4.59	1156	(Atkinson & Arey, 2003)	2.65	2012-2014
∑(*iso*, 1-Butene)	31.4[a]	938	(Atkinson & Arey, 2003)	0.31	2012-2014
cis-2-Butene	35.2	0	(Atkinson & Arey, 2003)	0.27	2012-2014
trans-2-Butene	0.000122	-382 (2)	(Atkinson & Arey, 2003)	0.22	2012-2014
cis-2-pentene	37	0	MCM	0.05	2012-2014
1-pentene	1.5	0	(Atkinson & Arey, 2003)	0.15	2012-2014
trans-2-pentene	37	0	MCM	0.09	2012-2014
1-Hexene	1.8	0	(Atkinson & Arey, 2003)	0.01	2012-2014
Alkynes					
Ethyne	0	0	MCM	7.58	2012-2014
Aromatics					
Benzene	0.003	0	(Atkinson & Arey, 2003)	1	2012-2014, 2017
Toluene	0.007	0	(Atkinson & Arey, 2003)	2.09	2012-2014, 2017
m-Ethyltoluene	0.045	0	MCM	0.11	2012-2014
o-Ethyltoluene	0.071	0	MCM	0.06	2012-2014
p-Ethyltoluene	0.086	0	MCM	0.05	2012-2014
Ethylbenzene	0.06	0	(Atkinson & Arey, 2003)	0.15	2012-2014
p-Xylene	0.050[b]	0	(Atkinson & Arey, 2003)	0.82	2012-2014, 2017

o-Xylene	0.041	0	(Atkinson & Arey, 2003)	0.25	2012-2014
m-Xylene	0.026	0	(Atkinson & Arey, 2003)	0.52	2012-2014
1,2,4-Trimethylbenzene	0.18	0	(Atkinson & Arey, 2003)	0.16	2012-2014, 2017
1,2,3-Trimethylbenzene	0.19	0	(Atkinson & Arey, 2003)	0.04	2012-2014
1,3,5-Trimethylbenzene	0.088	0	(Atkinson & Arey, 2003)	0.07	2012-2014
n-propylbenzene	0.014	0	MCM	0.03	2012-2014
iso-propylbenzene	0.014	0	MCM	0.01	2012-2014
Styrene	150	0	(Atkinson & Arey, 2003)	0.09	2012-2014
Biogenics					
Isoprene	315	450	(Atkinson & Arey, 2003)	0.02	2012-2014, 2017
MVK	0.06	0	(Atkinson & Arey, 2003)		2017
MACR	0.34	0	(Atkinson & Arey, 2003)		2017
Alcohols					
Methanol	94	2650	(Atkinson & Arey, 2003)		2017
Ketones					
Acetone	0.003	0	(Atkinson & Arey, 2003)		2017
MEK	0	0			2017
Pentanone	0	0			2017
Hexanone	0	0			2017
Aldehydes					
Acetaldehyde	140	1860	(Atkinson & Arey, 2003)		2017
Formaldehyde	0.056	0	(Atkinson & Arey, 2003)		2017

As the k_{NO_3} calculations in this analysis were based on ground-site measurements, k_{NO_3} values in each box model simulation were held constant at the value on each flight day at 4pm (values in
Table S3). Measured late afternoon concentrations at the ground within a mixed boundary layer are expected to be similar at night in the residual layer. For the flight on 18 January 2017, the PTR-MS was not measuring VOCs and the k_{NO_3} value was estimated by the growth rate of k_{NO_3} during the second PCAP event in Figure S1.

Table S3. Total k_{NO_3} values and initial VOC concentrations used model simulations

Flight Day	Total k_{NO_3} [s^{-1}]	Init. Conc. Styrene [molec. cm^{-3}]	Init. Conc. ∑(*cis, trans*-2-Butene) [molec. cm^{-3}]	Init. Conc. ∑(*cis, trans*-2-Pentene) [molec. cm^{-3}]	Init. Conc. Isoprene [molec. cm^{-3}]
18 Jan	9.5×10^{-3}	2.2×10^{9}	1.2×10^{10}	3.2×10^{9}	4.8×10^{8}
26 Jan	1.5×10^{-3}	3.5×10^{8}	1.8×10^{9}	5.1×10^{8}	7.6×10^{7}
28 Jan	4.4×10^{-3}	1.0×10^{9}	5.3×10^{9}	1.5×10^{9}	2.2×10^{8}
29 Jan	5.1×10^{-3}	1.2×10^{9}	6.3×10^{9}	1.7×10^{9}	2.6×10^{8}

One limitation of this method is that it does not allow the k_{NO_3} rate constant to vary with time, which is expected as VOCs are removed overnight in the RL by reaction with NO_3. To investigate the impact of time varying k_{NO_3} values on the model results, the top six contributing VOCs (Figure S1) (average 96% of the total reactivity) were represented semi-explicitly in the model using four additional reactions and second order rate constants given in
Table S1. The *cis*- and *trans*-isomers of 2-butene and 2-pentene were lumped in this analysis with the rate constants averaged between the two isomers. The initial concentrations of each VOC were taken as the concentrations at 4pm on the day of each flight (values in
Table S3). Allowing the VOC reactivity to be reduced overnight minimally impacted the model-derived nocturnal nitrate production rate (<0.1%), as shown discussed further in Section S1.4.

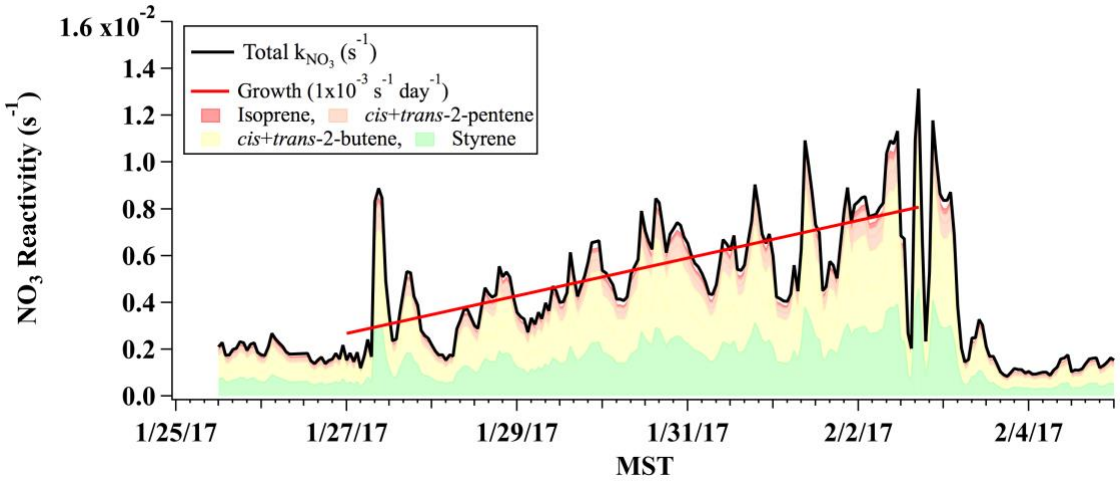

Figure S1. Time series of k_{NO_3} during the late January PCAP event (event #4) at the HW ground site in SLV. Total calculated k_{NO_3} is shown in black. The fractional contributions from the largest six contributing VOCs are shown in color. The PCAP k_{NO_3} growth rate is shown by the red line.

S1.3 Wet Surface Area Calculation

Total aerosol wet surface area (SA) density ($m^2\ m^{-3}$) was used to calculate $\gamma(N_2O_5)$ in Eq. (1) from the model-derived $k_{N_2O_5}$ loss rate constant. For the UWFPS campaign, the total wet SA (for particles < 1 μm in diameter) was estimated by applying a relative humidity-dependent, surface area hygroscopic growth curve to the dry PM_1 SA measured by the UHSAS aboard the TO. For base case simulations, the applied growth curve was calculated using the Extended-AIM Aerosol Thermodynamic Model (Wexler & Clegg, 2002), assuming no solid formation (i.e. metastable liquid particles) and pure NH_4NO_3 particles (Figure S2).

Alternatively, the growth factor for each point can be estimated from the aircraft AMS measurements, following supplemental Eqs. (S2) - (S5), as described further in McDuffie et al. (2018b). In these equations, V_{Dry} is the total dry aerosol volume measured by the UHSAS and V_{Total} is the sum of the dry and wet volume contributions. To assess the possible SA error associated with the assumption of pure NH_4NO_3 particles, V_{Wet} was calculated in (S3) from the mass of aerosol liquid water (M_{Wet}) and water density (ρ_{water}). M_{Wet} was calculated in (S4) as the sum of inorganic-associated water (calculated from ISORROPIA as described in Franchin et al. (2018)) and the organic-associated water, which was estimated in (S5) by the measured dry organic aerosol mass (M_{org}), organic density (ρ_{org}), water activity ($a_w = RH/100$), water density (ρ_{water}), and the organic hygroscopicity constant (κ_{Org}). While ρ_{org} and κ_{Org} have been shown to depend on multiple factors such as the aerosol O:C ratio (Cerully et al., 2015; Jimenez et al., 2009; Mei et al., 2013), ρ_{org} is set here to a constant value of 1.3 g/cm^3, typical of secondary organic aerosol (e.g. Kuwata et al., 2012) and κ_{Org} is set to 0.1 (Brock et al., 2016; Shingler et al., 2016).

Figure S2a shows the diameter growth curves (square root of the SA growth curves) as a function of RH for both the E-AIM and AMS estimates. As the aerosol in SLV are primarily composed of NH_4NO_3 during pollution events (Figure 4), the organic-associated water content has a small impact on the growth curve and total wet aerosol SA. The insert in Figure S2a shows that the wet SA only increases by ~ 3% when the organic-associated water is included in the growth factor calculation. Due to the small impact and large uncertainties associated with the calculation of organic-associated water, total wet SA and volume densities used in the main text include inorganic-associated aerosol water only. Figure S2b shows the distribution of measured dry and calculated wet aerosol surface area densities for points where $\gamma(N_2O_5)$ and $\phi(ClNO_2)$ values were derived from the box model.

$$Aerosol\ SA\ Growth\ Factor = \left(\frac{V_{Total}}{V_{dry}}\right)^{\frac{2}{3}} \quad \text{(S2)}$$

$$V_{Total} = M_{Wet}/\rho_{water} + V_{dry} \quad \text{(S3)}$$

$$M_{Wet} = M_{Inorg.\ water} + M_{Org.\ Water} \quad \text{(S4)}$$

$$M_{Org.\ Water} = \left(\frac{a_w}{1-a_w}\right) * \kappa_{Org} * \left(\frac{M_{org}}{\rho_{org}}\right) * \rho_{water} \quad \text{(S5)}$$

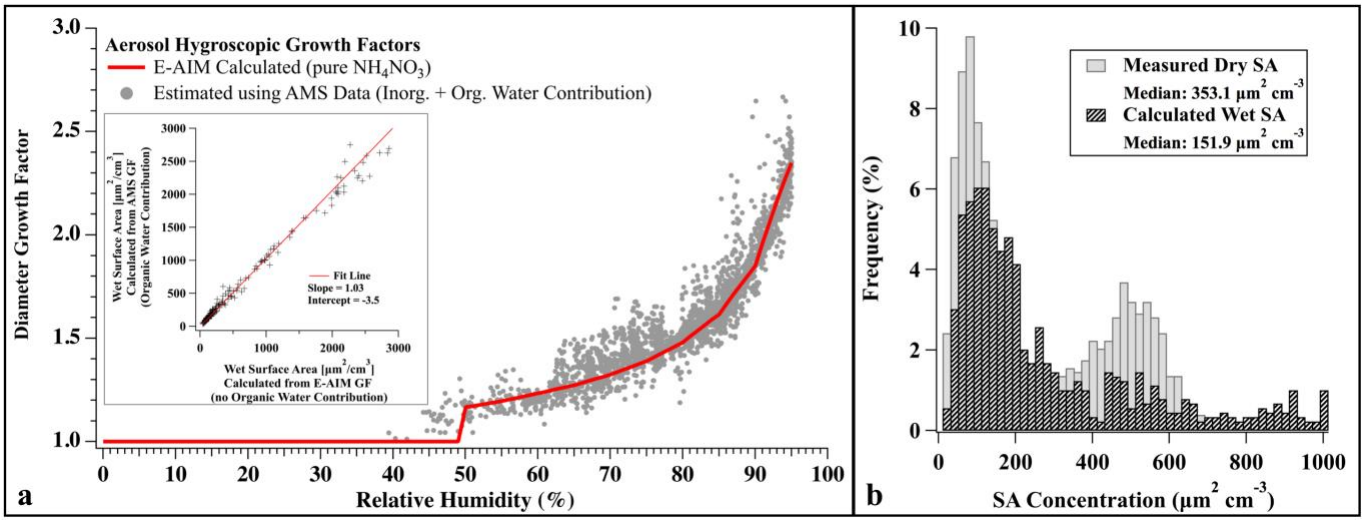

Figure S2. (a) Hygroscopic Diameter Growth Factors for <1μm diameter aerosol. (Red line) derived using E-AIM, assuming pure NH_4NO_3 aerosol and used for base case γ(N_2O_5) calculations, (gray circles) derived from Eqs. (S2) - (S5), using AMS data, including organic and inorganic-associated water. (Insert) Comparison of total wet SA during UWFPS, calculated using AMS and E-AIM growth factors. (b) Distributions of measured (dry) and calculated (wet) aerosol SA, with medians provided in figure caption. All data shown are from observation times with derived values of γ(N_2O_5) and ϕ($ClNO_2$) (N = 1031).

S1.4 Sensitivity Studies and Model Uncertainties

This section describes results of 17 additional simulations that were conducted to test the sensitivity of the model predicted nocturnal nitrate production rate (μg m^{-3} $night^{-1}$) to uncertainties in the box model inputs, constraints, and parameters. Results are summarized in Table S4 and Figure S3. Table S4 shows the percent change in the median nocturnal nitrate production rate and the number of points in each comparison. The number of points are different in each test as the model cannot always converge to a solution ($k_{N_2O_5}$ < 1×10^{-7} s^{-1} or k_{ClNO_2} > $k_{N_2O_5}$), as described in McDuffie et al. (2018b) and (McDuffie et al., 2018a). Non-converging points have been removed from this analysis. Figure S3 shows a time series of the nitrate produced overnight in base case simulations (black points), and the uncertainty associated with each point (shading). The uncertainty for each point was calculated from the quadrature addition of the percent changes associated with each of the sensitivity tests summarized in Table S4. The total absolute uncertainty is shown by the dark blue shading and the fraction of uncertainty associated with the incorporation of dilution is highlighted by light blue. An expanded view of data from 28 January is also shown for illustrative purposes. Individual sensitivity tests and results are described in further details in Sections S1.4.1– S1.4.2, discussed in decreasing order of model sensitivity.

Table S4. Median sensitivity of simulated nitrate to changes in model parameters.

Parameter	Base Case Value	Value Adjustment	ΔMedian Nocturnal Nitrate Production Rate (%)[a]	N
Dilution	n/a	$k_{dilution}$= 1.3×10^{-5} s^{-1}[b]	-42.4	1027
Deposition	n/a	k_{dep} = 2.6×10^{-6} s^{-1}[c]	+7.7	1027
NO_2	CRDS	+5%, -5%[d]	+5.7, -5.8	1021
O_3	CRDS	+5%, -5%[d]	+4.8, -4.8	1025
$ClNO_2$	I$^-$-ToF-CIMS	+30%, -30%[d]	-3.9, +4.3	1025
Photolysis Rates	WINTER values[e]	+40%, -40%	-1.4, +2.8	1809
N_2O_5	I$^-$-ToF-CIMS	+30%, -30%[d]	-1.0, +1.2	1021
Pre-Sunset Time	1.3 hours[f]	0 hrs, 2 hrs	-0.3, +0.2	505
Constant k_{NO_3}	Calculated[g]	+50%, -50%	-0.2, +0.2	1027
Varying k_{NO_3}	Constant k_{NO_3}	Varying k_{NO_3} [g]	<0.1	1027

[a]Defined as (base case value – sensitivity test value)/base case value *100
[b]See Section S1.4.1
[c]See Section S1.4.2
[d]Reported instrument measurement accuracies
[e]See Section S1.4.3
[f]See Section S1.4.4
[g]See Section S1.4.5

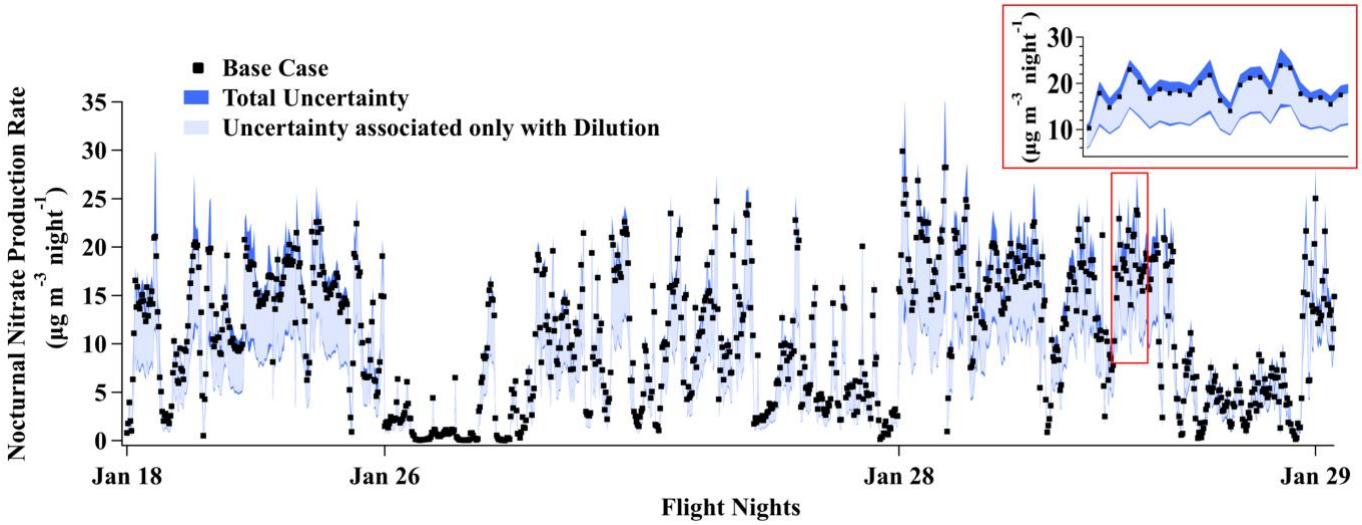

Figure S3. Time series of simulated nitrate production rate. Base case simulations are shown by black dots. The total uncertainty in each simulated point is given by the dark blue shading. Light blue shading shows the absolute uncertainty associated with the presence of dilution/mixing only ($k_{dilution}$= 1.3×10^{-5} s^{-1}). The insert shows a larger view of the region inside the red box.

S1.4.1 Dilution/Vertical Mixing

To test the box model sensitivity to the presence of vertical mixing/horizontal dilution, a first order loss rate constant of 1.3×10^{-5} s^{-1} was implemented into the chemical mechanism, as shown in Table S1. In addition to the first order loss of all simulated species, a constant 45 ppbv of background O_3 (average mixing ratio above the boundary layer during UWFPS) was added to the model with the same dilution rate constant to simulate the entrainment of O_3 into the RL from the free troposphere. The dilution rate constant was derived by Womack et al. (2018) (scaled up by 40% to represent the RL only), as the rate constant that, in combination with the derived surface albedo, allowed an observationally-constrained box model to best reproduce the diurnal profile of total O_x (= NO_2 + O_3 + 1.5*(HNO_3 + pNO_3^-) + 3*N_2O_5 + $ClNO_2$ + PANs + OH + 2*alkyl nitrates), that was observed between 28 and 31

January, 2017 at the HW ground site. Based on Figure S10 in Womack et al. (2018), the RL dilution rate constant could have reasonably ranged between 1.2 and 2.5×10^{-5} s^{-1} (0.7 -1.5×10^{-5} s^{-1} / 0.6), depending on the albedo. In the analysis presented here, the box model-predicted nocturnal nitrate production rate was most sensitive to this parameter, with a 42.2% reduction in the median predicted rate when including a dilution rate of 1.3×10^{-5} s^{-1}. Though uncertainties about ambient mixing processes in the RL remain, results incorporating estimated dilution rates are discussed further in Section 3.3.3 of the main text.

S1.4.2 Deposition

To estimate the effect of deposition on the amount of nocturnal nitrate produced by the model, an extra reaction was added to the mechanism where modeled nitrate (HNO_3) was lost with a first order rate constant of 2.6×10^{-6} s^{-1}. This rate constant was calculated assuming a gas-phase nitric acid deposition velocity of 2.7 cm s^{-1} (Zhang et al., 2012) and an average boundary layer height of 800m (determined from measured NO_y and PM vertical profiles). This deposition rate constant of 3.3×10^{-5} s^{-1} was reduced by 92% to account for the gas-particle partitioning of HNO_3 and particulate nitrate, modeled using the AMS and I^-ToF-CIMS data from the Twin Otter (Franchin et al., 2018). The presence of this small loss of gas-phase HNO_3 had a much smaller impact than dilution, with an increase in the median nocturnal nitrate production rate of 7.7%.

S1.4.3 Photolysis Rates

As described in the following section, each simulation was started 1.3 hours prior to sunset (as calculated from the solar zenith angle). In this analysis, photolysis rates during the 1.3 hours prior to sunset were calculated as a function of time prior to sunset from measurements of $j(NO_2)$, $j(O^1D)$, $j(N_2O_5)$, $j(ClNO_2)$, and $j(NO_3)$ during the 2015 WINTER aircraft campaign. During WINTER, photolysis rates were calculated form actinic flux measurements from the National Center for Atmospheric Research, High-performance Instrumented Airborne Platform for Environmental Research (HAIPER) Airborne Radiation Package – Actinic Flux (HARP-AF) HARP-AF instrument (Shetter & Müller, 1999). These radiative measurements have an increased uncertainty of up to 40% near sunset at large solar zenith angles, which exacerbate the optical angular response biases. Accounting for this source of uncertainty, the nocturnal nitrate production rate over SLV during the UWFPS campaign changed by -1.4/+2.8% for +/- 40% changes in photolysis rates.

S1.4.4 Pre-Sunset Time

Simulations were set to begin before sunrise to account for the observed build-up of N_2O_5 and $ClNO_2$ at large solar zenith angles. The value of 1.3 hours was derived from the 2015 WINTER campaign as the time when ambient observations of N_2O_5 deviated from the values predicted by the daytime steady state approximation of N_2O_5 (Brown et al., 2005) (Eqs. (S6) and (S7)). This value could not be recalculated for the UWFPS campaign as it requires measurements of $j(NO_3)$. During the WINTER campaign, this "pre sunset" time was found to vary between 0.8 to 1.8 hours. In this analysis, the box model was tested by changing the start time of each simulation to 0 and 2 hours prior to sunset. Of the points that converged, the median nocturnal nitrate production rate changed by < 0.3% for both tests.

$$[NO_3]_{\text{daytime ss}} = \frac{k_1[O_3][NO_2]}{k_7[NO] + j(NO_3)} \quad \text{(S6)}$$

$$[N_2O_5]_{\text{daytime ss}} = \frac{k_{2f}}{k_{2r}}[NO_2][NO_3]_{\text{daytime ss}} \quad \text{(S7)}$$

S1.4.5 NO_3 Reactivity, k_{NO_3}

In the base case simulations, first order reaction rate constants were held constant for the NO_3 + VOC reaction. As described in Sections 2.2.2 and S1.2, values of k_{NO_3} were held constant throughout each simulation at values equivalent to the concentrations calculated for 4pm at the HW ground site (Figure S1). Due to uncertainties in the VOC measurements, the possible presence of non-measured VOCs and/or HO_2 or RO_2 radicals, and lack of measurements in the residual layer, sensitivity studies were conducted with k_{NO_3} values scaled by ± 50%. The median model predicted nocturnal nitrate production rate changed by 0.2% with ± 50% changes in constant k_{NO_3}.

As mentioned in Section S1.2, applying a constant k_{NO_3} does not allow for the potential decrease of k_{NO_3} overnight as VOCs are consumed by reaction with NO_3. To test the model sensitivity to this variable process, the six largest contributing VOCs to k_{NO_3} (average 96% of the total reactivity) were represented semi-explicitly in model simulations, as shown in

Table S1. These six VOCs were styrene, *cis*-, *trans*-2-butene, *cis*-, *trans*-2-pentene, and isoprene. The average of *cis* and *trans* isomers were used to minimize the number of additional reactions in the model mechanism. Initial concentrations of each VOC for each flight are listed in

Table S3 and were taken from the 4pm values on each flight day. Allowing the total k_{NO_3} to vary overnight changed the median nocturnal nitrate production rate by <0.1%.

Section S2 $P_{NO_3^-}$ Calculation Details

The instantaneous nitrate production rate ($P_{NO_3^-}$) is calculated as two times the production rate of N_2O_5 ($P_{N_2O_5}$). $P_{N_2O_5}$ (sometimes reported as P_{NO_3}) is calculated from the first order reaction of O_3 + NO_2, which is the rate limiting step in the formation of NO_3, which forms an equilibrium with N_2O_5 at night. $P_{N_2O_5}$ is calculated in units of molec. cm^{-3} s^{-1} but is frequently reported in units of ppbv hr^{-1} after it is converted using the ambient air number density (ND) and the conversion between seconds and hours (3600) and mixing ratio to ppbv. In in Section 3.3.1 of this analysis, $P_{N_2O_5}$ is further converted to units of μg m^{-3} hr^{-1}, shown below in Eq. (S8), in order for $P_{NO_3^-}$ to have consistent units with the aerosol concentration measurements and box model results.

$$P_{N_2O_5}\ [\mu g\ m^{-3}\ hr^{-1}] = P_{N_2O_5}\ [ppbv\ hr^{-1}] * 1 \times 10^{-9} * ND\ [molec.\ cm^{-3}] * \frac{1}{6.022 \times 10^{23}\ [molec.\ mol^{-1}]} * 62\ [g\ mol^{-1}]\ NO_3 * 1 \times 10^{12}\ [\mu g\ cm^3\ g^{-1} m^{-3}] \quad \text{(S8)}$$

Section S3 Additional Figures

As noted in the main text, O_3 measurements at the HW ground site were corrected for an apparent offset in the data prior to a 2-hour data gap on 23 January 2017. As shown in Figure S4, the O_3 at HW becomes fully titrated during pollution episodes after the 23rd. Prior to 23 January, the O_3 data have the same apparent titration during pollution events but reach a minimum of ~ 4.5 ppbv.

The O_3 data during this time were therefore reduced by a constant 4.5 ppbv to bring these data into agreement with 0 ppbv during pollution episodes. No adjustments were made to the data span during either time period.

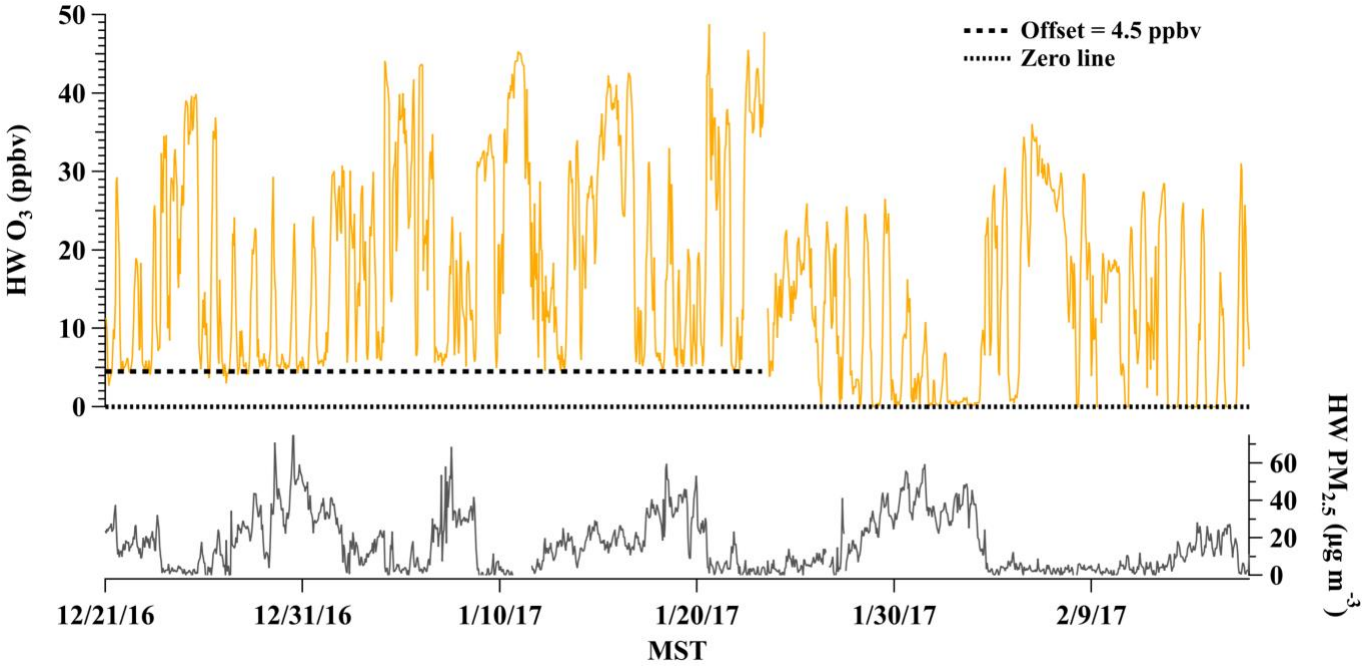

Figure S4. Time series of measured HW $PM_{2.5}$ (bottom) and O_3 (top), highlighting the O_3 offset correction of 4.5 ppbv

Section S4 $\gamma(N_2O_5)$ and $\phi(ClNO_2)$ Derivation Method Details

S4.1 Steady State Approximation for $\gamma(N_2O_5)$

The nocturnal steady state lifetime of N_2O_5 ($\tau_{ss}(N_2O_5)$) has been previously defined by Brown et al. (2003) and is shown in Eq. (S9) as a steady state between N_2O_5 production and nocturnal destruction pathways. Substituting the expression in Eq. (1) for $k_{N_2O_5}$, Eq. (S9) can be rearranged into to Eq. (S10) to solve for the steady state approximation of N_2O_5 uptake ($\gamma_{ss}(N_2O_5)$). This method for estimating the N_2O_5 uptake coefficient is simple relative to the box model but can fail under cold temperatures, high NO_2 concentrations, and small sinks for both N_2O_5 and NO_3 (Brown et al., 2003). Figure S5 shows that agreement between the box model and steady state approximation was within 19% (2-sided slope) over SLV during the UWFPS campaign.

$$\tau_{ss}(N_2O_5)^{-1} = \frac{k_1[NO_2][O_3]}{[N_2O_5]} \approx \left(k_{N_2O_5}\right) + \frac{k_{NO_3}}{K_{eq}[NO_2]} \quad \text{(S9)}$$

$$\gamma_{ss}(N_2O_5)0.25cSA = \frac{k_1[NO_2][O_3]}{[N_2O_5]} - \frac{k_{NO_3}}{K_{eq}[NO_2]} \quad \text{(S10)}$$

S4.2 $\gamma(N_2O_5)$ and $\phi(ClNO_2)$ Parameterizations

Box model values were also compared to $\gamma(N_2O_5)$ and $\phi(ClNO_2)$ values predicted from the parameterizations presented by Bertram and Thornton (2009), provided in Eqs. (S11) and (S12).

$$\gamma(N_2O_5) = \frac{4}{c}\frac{V}{SA} K_H * \beta * (1 - e^{(-\delta[H_2O(l)])}) \left(1 - \frac{1}{\left(\frac{0.06[H_2O(l)]}{[NO_3^-]}\right) + 1 + \left(\frac{29[Cl^-]}{[NO_3^-]}\right)}\right) \quad \text{(S11)}$$

$$\varphi(ClNO_2) = \frac{1}{\left(1 + \frac{[H_2O(l)]}{483[Cl^-]}\right)} \quad \text{(S12)}$$

Here, c (m s^{-1}) is the mean molecular speed, SA is the total wet aerosol SA (discussed in Section S1.3), and V is the total wet aerosol volume (m^3 m^{-3}). Here, V was calculated using the UHSAS-measured dry aerosol volume density and the inorganic-associated aerosol water mass (discussed above in Section S1.3). The constants β (1.15 $\times 10^6$ [s^{-1}]), δ (0.13 [M^{-1}]), 0.06, and 29, and 483 were derived from fits to laboratory results presented by Bertram and Thornton (2009). . K_H is the unitless Henry's Law Coefficient of 51, taken from (Fried et al., 1994). Aerosol water molarity was calculated using ISORROPIA-predicted aerosol water mass and V. This estimate does not include aerosol mass associated with organic-associated aerosol water, which is estimated to be a relatively small fraction of total aerosol water (3-17%) due to the small dry mass fraction of aerosol organics (~20%, Figure 4). Aerosol chloride and nitrate molarities were calculated from AMS nitrate and chloride mass measurements and V. Comparisons of these parameterizations to the box model results are shown in Figure S5 and discussed in the main text.

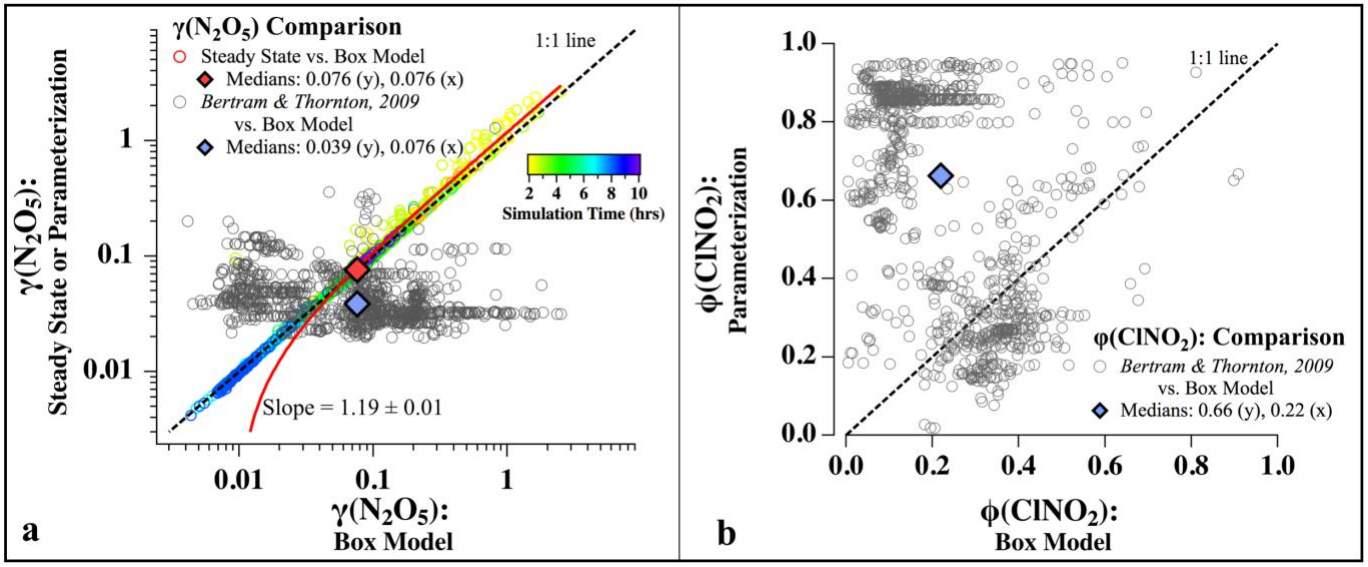

Figure S5. Methods comparison for $\gamma(N_2O_5)$ and $\phi(ClNO_2)$ values during pollution events in SLV. (Left) Colored circles show the comparison between steady state (y-axis) and box model (x-axis) derived $\gamma(N_2O_5)$ values, colored by model simulation duration (i.e. time since sunset). The 2-sided fit produces a slope of 1.19 ± 0.01, shown by the red line. (Left & Right) Gray circles show the comparison between parametrized values (from Bertram and Thornton (2009)) (y-axis) and box model (x-axis) results. Dashed lines show the 1:1 line. Medians of each derivation are shown by diamonds and labeled accordingly.

As mentioned in the main text, the median $\gamma(N_2O_5)$ was also predicted by an empirically-derived parameterization (S13) (McDuffie et al., 2018b). Details of this parameterization can be found in McDuffie et al. (2018b). For estimations here, the O:C ratio was calculated using the improved-ambient O:C ratio method from Canagaratna et al. (2015), shown in (S14). The AMS organic mass fragment at *m/z* 44 (f_{44}) ranged between 0.05 and 0.25 during UWFPS (Figure 6, Franchin et al. (2018)), corresponding to an O:C ratio between ~0.3 and 1.16. Additional parameters include R_p, R_c, and ℓ, which are the total particle radius, radius of the inorganic core, and thickness of the organic coating, respectively. Here R_p was take as the effective aerosol radius, while R_c was calculated from the inorganic/(organic + inorganic) volume fraction following the equations presented in Table S8 of McDuffie et al. (2018b),

based on Riemer et al. (2009). The organic volume required for this calculation was estimated using a constant organic density of 1.3 g/cm^3. In addition to the same variables as described above, R is the ideal gas constant, T is the ambient temperature and H_{aq} (5000 mol m^{-3} atm^{-1}) (Anttila et al., 2006) and D_{aq} (1x10^{-9} m^2 s^{-1}) (Riemer et al., 2009) are the aqueous N_2O_5 solubility and diffusion rate constants, respectively. With the assumptions described here, the median uptake coefficient predicted by this parameterization was estimated to be between 60 and 85% lower than the box model for O:C ratios between 0.05 and 1.16. As this parameterization treats the presence of organics as a coating that is resistive to uptake, the under-estimation of $\gamma(N_2O_5)$ relative to the box model may indicate: 1) aerosol organics during pollution events are not surface active, 2) organics are not resistive toward N_2O_5, or 3) box model $\gamma(N_2O_5)$ values are over-predicted due to missing SA (Section 3.3.2, e.g. fog) or simplifying assumptions discussed in Sections 2.2.2 and 3.3.2 (e.g. dilution). Due to uncertainties, these results are not assessed further.

$$\frac{1}{\gamma} = \frac{1}{\frac{4}{c}\frac{V}{SA}K_H * 2.14 \times 10^5 * [\mathrm{H_2O}(l)]\left(1 - \frac{1}{\left(\frac{0.04[\mathrm{H_2O}(l)]}{[\mathrm{NO_3^-}]}\right)+1}\right)} + \frac{1}{\frac{4RT(0.15 * O{:}C + 0.0016 * RH) * H_{aq}D_{aq}R_c}{c\ell R_p}} \quad \text{(S13)}$$

$$\text{Aerosol O:C} = 0.079 + 4.31 * f_{44} \quad \text{(S14)}$$